Functional Nanostructured Materials (including low-D carbon)

WSe Homojunction p-n Diode Formed by Photo-induced Activation of Mid-gap Defect States in Boron Nitride

Sikandar Aftab, Imtisal Akhtar, Yongho Seo, and Jonghwa Eom

ACS Appl. Mater. Interfaces, **Just Accepted Manuscript** • DOI: 10.1021/acsami.0c12129 • Publication Date (Web): 20 Aug 2020

WSe_2 Homojunction p-n Diode Formed by Photo-Induced Activation of Mid-Gap Defect States in Boron Nitride

Sikandar Aftab[1], Imtisal Akhtar[2], Yongho Seo[2] and Jonghwa Eom[1]*

[1]Department of Physics & Astronomy and Graphene Research Institute-Texas Photonics Center International Research Center (GRI-TPC IRC), Sejong University, Seoul 05006, Korea

[2]Department of Nanotechnology & Advance Materials Engineering, Sejong University, Seoul 05006, Korea

*E-mail: eom@sejong.ac.kr

KEYWORDS: Photo-induced doping, homojunction p-n diode, h-BN, WSe_2, h-BN

ABSTRACT: A single nanoflake lateral p-n diode (in-plane) based on a two-dimensional (2D) material can facilitate electronic architecture miniaturization. Here, a novel lateral homojunction p-n diode of a single WSe_2 nanoflake is fabricated by photo-induced doping via optical excitation of defect states in an h-BN nanoflake upon illumination. This lateral diode is fabricated using a mechanical exfoliation technique by stacking the WSe_2 nanoflake partially on the h-BN and Si substrate. The carrier type in the part of WSe_2 film on the h-BN substrate is inverted and a built-in potential difference is formed, ranging from 5.0 to 4.50 eV, which is measured by Kelvin probe force microscopy. The contact potential difference across the junction of p-WSe_2 and n-WSe_2 is found to be ~492 mV. The lateral diode shows an excellent rectification ratio, up to ~3.9×10^4 with an ideality factor of ~1.1. A typical self-biased photovoltaic behavior is observed at the p-n junction upon the illumination of incident light, a positive open-circuit voltage (V_{oc}) is generated i.e. voltage obtained (at $I_{ds} = 0$ V) and also a negative short-circuit current (I_{sc}) i.e. current obtained (at $V_{ds} = 0$ V). The presence of built-in potential in the proposed homojunction diode establishes I_{sc} and V_{oc} upon illumination, which can be implemented for a self-powered photovoltaic system in future electronics. The proposed doping technique can be effectively applied to form planar homojunction devices without photoresist for future electronic and optoelectronic applications.

INTRODUCTION

The family of two-dimensional (2D) layered transition metal dichalcogenides (TMDs) shows a wide range of characteristics in terms of intrinsic doping and band structures, allowing their application in various electronic and optoelectronic nanodevices. [1-4] These ultra-thin 2D layered materials may replace the conventional Si-based complementary metal-oxide-semiconductors (CMOSs) and facilitate structural flexibility and miniaturization in the development of transparent electronic devices [5] for the next-generation applications. [6] Among the TMD-based 2D materials, tungsten diselenide (WSe_2) is a popularly emerging material owing to its comparatively high hole mobility (μ), approximately 100–250 cm^2 /V s with an excellent on/off ratio of ~10^7. [7-10] WSe_2 can be exfoliated (into a monolayer or multi-layers) from its bulk form using a mechanical exfoliation technique with an adhesive tape. A monolayer of WSe_2 shows a direct bandgap of ~1.7 eV, while its bulk form shows an indirect bandgap of ~1.0 eV. [11]

The TMD family offers unprecedented design flexibility in creating p-n junction devices which is not possible using conventional bulk semiconductor materials. [12-13] Until now, TMD-based p-n diodes have been exclusively prepared by stacking 2D materials, forming homostructures or heterostructures. Many researchers have implemented various doping approaches such as surface charge transfer, chemical doping, substitutional doping, surface functionalization, electrostatic gating, and intercalation with complicated device structures to prepare lateral homojunction diodes. [12, 14-19] However, such devices contain non-abrupt interfaces due to the use of photoresist, also they experience degeneration of electrical properties due to chemical or environmental effects which confine the necessary operation. [24-27]

Charge conversion was demonstrated in graphene using electrostatic doping, but it could not establish diode-like behavior due to the zero-band gap with Klein tunneling. [20] Enabling n- and

p-type behaviors in the same nanoflake of 2D materials is difficult as it often requires doping engineering techniques, such as electrostatic gating, elemental effect, and unstable chemical treatment. [21-23]

An insulating 2D material, hexagonal boron nitride (h-BN) is recently receiving attention, owing to its properties like good mechanical strength, extraordinary thermal conductivity (due to the strong B-N covalent bonds in its plane), along with excellent thermal and chemical stability. [5, 28] It exhibits an extremely low value of permittivity (ε) of 3.6–5.3 due to the strong covalent nonpolar bonds. [29] Like WSe_2, h-BN can also be exfoliated into a multi-layer from the bulk crystals and used as a dielectric substrate, which has been effectively confirmed from the so-called "graphene plus further TMD field-effect transistors (FETs)." [30-31] Under DUV light illumination h-BN exhibits a bright excitonic luminescence verified by photoluminescence measurements. [32] The existence of defect states or point defects in h-BN has been confirmed by a rich array of sub-band-gap luminescence lines originated from the recombination at impurities or native defects. [33]

In this research, we developed a lateral WSe_2 based homojunction p-n diode, where the p-type WSe_2 nanoflakes exhibit an efficient doping effect using the optical excitation of mid-gap donor-like states (or defect states)[34] in multilayered h-BN nanoflakes i.e., to exploit photo-induced electron transferred from defects in h-BN to adjacent WSe_2 and establish n-type doping effect. Lateral WSe_2 homojunction p-n diodes are fabricated by the vertical stacking of WSe_2 nanoflakes on the h-BN and silicon dioxide substrates (SiO_2) partially, using dry transfer method. The mechanism of the electron carrier type modulation in WSe_2 nanoflake under photo-induced doping, is analogous to the carrier type modulation in those heterostructures, that are composed of graphene and h-BN or WSe_2/SiO_2. [35-37] This photo-induced effect of ultrafast carrier modulation in the heterostructures of WSe_2 and h-BN is due to the mid-gap of donor-like states in the h-BN

flakes. However, the photo-induced effect observed in graphene nanoflakes that were exfoliated on thick SiO_2 substrates, originating from the interfacial trapped states of charges in amorphous oxide. [38] We have confirmed that the FETs based on p-WSe_2 are inverted to the n-type conduction that preserves efficient electron carrier mobility in the heterostructures of h-BN and n-WSe_2. To further verify the photo-induced doping mechanism, Kelvin probe force microscopy (KPFM) experiments were implemented and discovered that the Fermi level of p-type WSe_2 nanoflake was satisfactorily modified to that of an n-type WSe_2. The proposed lateral WSe_2 homojunction diode shows outstanding electronic and optoelectronic characteristics.

RESULTS AND DISCUSSION

The ultra-thin h-BN and WSe_2 nanoflakes were prepared by the standard mechanical exfoliation technique with an adhesive tape. Stacked h-BN/WSe_2 heterostructures were fabricated using the dry transfer method. The optical microscopy image of the h-BN/WSe_2 heterostructure based FETs is shown in Figure 1(a). The WSe_2/h-BN heterostructure was illuminated by DUV light (Figure 2(b)). The p-type WSe_2 flake on h-BN is altered to the n-type WSe_2, upon the exposure to deep ultra-violet light (DUV) illumination with a photon energy of ~5.63 eV and an applied gate voltage of −40 V.

Figure S1 (a, b) in Supporting Information, shows the micro-Raman spectra for both h-BN and WSe_2 nanoflakes. We achieved the Raman spectroscopy of WSe_2 multilayered BN nanoflakes using a setup which has an excitation laser (514 nm, 2.41 eV). Typically, the Raman peaks for WSe_2 (A_{1g} mode at ~261.2 /cm and E_{2g}^1 mode at ~250.6 /cm) and h-BN (E_{2g} mode at ~1364.1 /cm) were observed. Figure S2(a) displays AFM images of the WSe_2 and h-BN nanoflakes

and the AFM profile height line scan is shown in Figure S2 (b, c). The h-BN and WSe_2 nanoflakes have thicknesses, ~15 and ~4 nm, respectively.

Figure 1 (a) shows the fabricated FET based heterostructures of the h-BN and p-type WSe_2 nanoflakes. The pristine p-type WSe_2 mostly exhibited the p-type behavior as confirmed from transfer characteristics as shown in Figure 1 (b). The metal contacts, Pd/Au attached to the source and drain exhibit pure ohmic behavior, which can be seen in the I_{ds}-V_{ds} characteristics as shown in Figure S3 (a). When the h-BN/p-type WSe_2 heterostructure is illuminated under the photon energy of 5.6 eV for 5 minutes with an applied gate voltage of −20 V, a photo-induced doping effect is achieved. The applied gate voltage (V_g^{light}) is a back-gate voltage, which is applied during the illumination of DUV or visible light to make the photo-induced doping effect. The doped WSe_2 flakes showed the n-type behavior as confirmed from the transfer characteristics (Figure 1 (b)), while the metal contacts (Pd/Au) attached to the source and drain exhibit a non-ohmic behavior, which is confirmed from the I_{ds}-V_{ds} characteristics as shown in the Figure S3 (b) of supporting information. The n-type WSe_2 flake showed rectifying behavior with Pd/Au electrodes. The WSe_2 with metal (Pd) can display either a unipolar p- or n-type transport curve or an ambipolar type conduction.

To confirm the hypothesis of photo-induced doping mechanism, the KPFM experiments were conducted to find the exact values of work function before and after the photo-induced doping of WSe_2 flakes. The following equation is used to find the work function of p- or n-type WSe_2:

$$e \times CPD = \phi_{sample} - \phi_{tip} \qquad (1)$$

where ϕ_{Sample} and ϕ_{tip} are the individual values of the work function of the sample and tip. The contact potential difference (CPD) of the reference HOPG (highly ordered pyrolytic graphite,

$\phi_{HOPG} = 4.6\ eV$) surface was −100 mV, which confirmed that $\phi_{tip} = 4.7\ eV$. The CPD of p-WSe_2 was 300 mV, which made the work function of WSe_2 for its pristine state (ϕ_{P-WSe_2} = 5.0 ± 0.08 eV). For the n-type WSe_2, the CPD was approximately −200 mV. Therefore, the work function of n-type WSe_2 is ϕ_{n-WSe_2} = 4.5 ± 0.10 eV.

The photo-induced mechanism of electron doping in the heterostructures of h-BN and WSe_2 flakes is caused by the optical excitation of mid-gap donor-like states (or defect states) in h-BN upon the illumination by light. The photons of deep UV light can excite the donor-like defect states [39] in h-BN (Figure 1 (c, d)), which demonstrates the physical mechanism of the photo-induced effect of carrier modulation in the heterostructures of WSe_2 and h-BN. Upon illumination by the deep UV light, the electrons of mid-gap defect states in the h-BN are excited (or triggered) to the conduction band by the energy of incident photons. The photon-excited electrons enter the WSe_2 flake under negative gate voltage. The positively charged localized ionized defects in h-BN reduce the influence of the external electric field (i.e., V_g^{light}) on h-BN during the photo-induced effect. This removal process continues till the external electric field across the h-BN disappears and the positively ionized defects remain inside the h-BN. [39] These positively charged defects are stored in the h-BN even after the removal of light and the V_g^{light}, which leads to the stable doping effect in WSe_2. We have also studied the dependence of the doping effect of the photon energy of illumination. The heterostructures of h-BN and WSe_2 were illuminated by the visible light (λ = 600 nm, 400 nm, 20 mW/cm^2) and deep UV light (λ = 220 nm, 11 mW/cm^2) with V_g^{light}= −40 V for 5 minutes. In all these cases, the doping effect was established in WSe_2, which revealed that the mid-gap defects could be excited upon the illumination by visible light, but we found that better

doping effect was achieved by the DUV light of photon energy, 5.63 eV with V_g^{light}= −40 V and 5 min of illumination (Figure S4).

The photo-induced electron doping in WSe_2 nanoflakes eliminates the need for complicated device architectures (using various photoresists) to modulate the carrier type in 2D materials. [40-41] Furthermore, the photo-induced doping is simple to apply on the WSe_2 FETs based on mechanical exfoliation, since this process did not affect the properties of metal contacts in the device. Consequently, this approach of electron doping is superior to previous artificial doping methods, such as doping through electrostatic gating effect to amend the carrier type concentration, [42] with different metal contacts to enable unipolar p- or n-type conduction in a similar nanoflake, or electrostatic doping in a planar device. [21-23]

We have found that the electron doping effect in WSe_2 depends on V_g^{light}, which means that on-current on electron regime increased with a rise in V_g^{light}. The electronic carrier concentration $n_{(n-WSe_2)}$ for the V_g^{light}can be calculated using the following relation:

$$n_{(n-WSe_2)} = -C_g (V_{bg} - V_{th})/e, \qquad (2)$$

where V_{bg} is the back gate voltage, V_{th} is the threshold voltage for electron transport, e is the electronic charge, and C_g is the gate capacitance/unit area for thick SiO_2 film with 300 nm, its value is ~115 × 10^{-10} F/cm^2. The value of C_g for h-BN is calculated by $C_g = \varepsilon_0\varepsilon_r/d$, where ε_0 = vacuum permittivity, d = thickness of h-BN, and ε_r = dielectric constant of h-BN, which equals 4. [43] For h-BN nanoflake having a thickness of 15 nm, the C_g is ~2.36 × 10^{-7} F/cm^2, and the combined gate capacitance is ~1.09× 10^{-8} F/cm^2. For example, at V_{bg} = −60 V, $n_{(n-WSe_2)}$ was calculated to be ~3.27 × 10^{12} cm^{-2}. The electron concentration is estimated to be 2.05 × 10^{12} cm^{-2} after photo doping under V_g^{light} = −10 V. Further increasing V_g^{light} to −60 V, the electron concentration is

increased to 3.28 × 10^{12} cm^{-2}. The larger value of V_g^{light} facilitates the formation of positively charged defects in higher concentration, localized in the mid-gap donor-like states (or point defects) in the BN flake,[39] which makes the electron-doping effect more efficient and enhances the electron concentration in the n-WSe_2/BN FET device.

The field-effect mobility $\mu_{(n-WSe_2)}$of n-type WSe_2 FET can be found by the following equation, [44]

$$\mu_{(n-WSe_2)} = \frac{L}{W}\left(\frac{dI_{ds}}{dV_{bg}}\right)\frac{1}{C_g V_{ds}} , \quad (3)$$

where *L* and *W* are the dimensions of n-type WSe_2 flake, its length and width, respectively, and $\left(\frac{dI_{ds}}{dV_{bg}}\right)$ is the slope of the transfer plot in the linear region. For example, $\mu_{(n-WSe_2)}$ of n-WSe_2 based FET was estimated as ~77.5 $cm^2V^{-1}s^{-1}$ after applying V_g^{light} = −60 V. The photo doping effect in the n-WSe_2/BN FET device exhibits the strong enhancement of electron mobility, from 9.7 to 77.5 cm^2 V^{-1} s^{-1} with increasing the V_g^{light} from −10 to −60 V. The carrier concentration $n_{(n-WSe_2)}$ and electron mobility $\mu_{(n-WSe_2)}$ as a reference to varying $V_g^{light}$are shown in Figure 1 (f). Moreover, we found that our results regarding the carrier concentration and electron mobility are either better or on a par with the previous reports based on different doping mechanisms. [45-49]

Additionally, we did not notice any clear peak shift of WSe_2 after the photo-induced effect at $varied\ V_g^{light}$, and there was no added Raman peak, inferring that the photo-induced doping technique did not produce extra effects in the WSe_2 nanoflake (Figure S5). Also, we did not find any disintegration in the electrical characteristics of the device even after retaining it in an ambient environment for several days. The prepared WSe_2 flakes have shown a stable n-type doping effect in the ambient environments (Figure S6).

We have demonstrated the preparation of the lateral WSe_2 homojunction p-n diode using a mechanical exfoliation technique by stacking the nanoflakes of WSe_2 on a multilayered h-BN flake, where a portion of the WSe_2 flake was placed on an h-BN, and the remaining area was placed on an Si/SiO_2 as shown in the Figure 2 (a). Figure 2 (b) demonstrates the optical microscope image of the device. Figure 2 (c) shows the difference between WSe_2/SiO_2 and WSe_2/h-BN parts of a single WSe_2 flake before the doping process. The CPD of WSe_2 flakes on the SiO_2 and h-BN substrates is ~46 mV before photo doping as shown in Figure 2 (d), which is probably caused by the interface trap charges on the SiO_2 substrate. The work function difference between the WSe_2/SiO_2 and WSe_2/h-BN before doping was 0.06 eV. The difference between pristine WSe_2/SiO_2 and doped WSe_2/h-BN parts of a single WSe_2 flake can be seen in the Figure 2 (d).

The heterostructure of h-BN and WSe_2 was illuminated upon the exposure to the deep UV light (λ = 220 nm, 11 mW cm^{-2}). Only the part of the p-type WSe_2 flake on h-BN was inverted to the n-type WSe_2 by the DUV illumination for 5 minutes with the photon energy ~5.6 eV at $V_g^{light} = -40$ V. After the doping process, we measured the CPD across the junction of n-WSe_2 and p-WSe_2. The CPD value from the KPFM image is given by the line scan indicated in Figure 2 (e), which gives the value of CPD at ~492 ± 8.48 mV as shown in Figure 2 (f). In this case, the value of CPD is higher than the previously reported planar diode (~55 meV) achieved by helium ion irradiation, [50] and the $MoTe_2$-based homojunction diode (~100 meV) achieved through deep UV light in an N_2 gas environment.[51]

To achieve low-resistance metal contacts, Pd/Au and Al/Au with the thickness of 6/100 nm were deposited on the p-WSe_2 and n-WSe_2 flakes, respectively. The work function of Pd (~5.2 eV) [52] is slightly greater than the valence band maximum or the Fermi level (5.0 eV) of p-WSe_2. Conversely, the work function of Al electrodes is ~4.1 eV [53] which is smaller than the electron

affinity (~4.21 eV) of n-type WSe_2. The *I-V* characteristics of both p-WSe_2 with Pd/Au metal contacts and n-WSe_2 with Al/Au contacts show an ohmic behavior (Figure S7 (a, b)), and their transfer characteristics show the p- and n-type conductions, respectively (Figure 3 (a)). We evaluated the rectifying behavior of lateral WSe_2 p-n diode by varying the gate voltage (V_{bg}) from +40 to −80 V. As V_{bg} increases from −80 to −30 V, the diode current decreases rapidly in the reverse bias as shown in Figure 3 (b), yielding to an increase in the rectification ratio (forward to reverse currents, I_f/I_r, at ±2 V) up to ~3.9×10^4 (Figure 3 (c)). We repeated the experiments and found that the uncertainty in the rectification ratio of devices remains 39000 ± 80. We compared the performance of our p-n diode with the previous reports (using other doping methods) such as elemental doping effect, [54-55] chemical doping, [18, 45] and doping due to electrostatic gating [56-57] as shown in Figure 3 (e). The rectification ratio of our device exhibits a better performance than the previously reported $MoTe_2$ based p-n diode. [51] When V_{bg} increases further from −30 to +40 V, the reverse current ($V_{ds} < 0$) becomes nearly constant, but the diode current in the forward bias regime ($V_{ds} > 0$) continues to decline, resulting in a decay of the p-n diode rectification ratio as shown in Figure 3 (c). We also examined the rectification ratio using different asymmetric contacts of the pristine WSe_2 flake without the photo-induced doping. The rectification ratio of (Pd/Au)-(p-WSe_2)-(Al/Au) device was ~22.6 at V_{bg} = 0 V as shown in Figure S8. However, the WSe_2 p-n diode was properly formed after the photo-induced doping and the diode rectification ratio was ~1.22×10^4 at V_{bg} = 0 V (Figure 3 (c)).

The ideality factor of the lateral WSe_2 p-n diode was extracted by the following equation:

$$I_D = I_O\left[exp\left(\frac{e\,V}{nK_BT}\right) - 1\right], \qquad (4)$$

where I_D is the diode current (i.e. I_f), I_O is the reverse saturation current (i.e. I_r at saturation), V is the applied voltage across the diode during its action, K_B = Boltzmann constant, and T = 300 K. The lower value ideality factor n was 1.1 at $V_{bg} = -30$ V (Figure 3 (d)). In our case, the ideality factor is better than the previously reported p-n junctions. [18, 38, 58-60] The rectifying behavior of the lateral homojunction p-n diodes regarding the gate voltages originates from the modification of the built-in potential at their homointerface of the p-WSe_2 and n-WSe_2 by an electric field. In Figure 4 (a), the transfer curve (I_{sd}-V_{bg}) can be categorized into four regions. This infers that the WSe_2 homojunction diode possesses the four junction types pp^+, pn^-, p^-n, and nn^+. In the pp^+ regime, the Fermi level of both p-WSe_2 and n-WSe_2 channels shifts down to the valence band under the greater negative back gate voltage, such that the holes become dominant in both p-WSe_2 and n-WSe_2 channels as shown in Figure 4 (b, i), and the device exhibits p-type semiconducting characteristics. Further by increasing the back gate voltage (i.e. rise in voltage from negative to a positive value), the Fermi level shifts near the bandgap and forms either a pn^- or p^-p junction state, as a result of the built-in potential at their homointerface, causing an increase in the rectification ratio as shown in Figure 4 (b, ii, iii). When the gate voltage was greater enough, the Fermi level moved into the conduction band in both p-WSe_2 and n-WSe_2 channels, where the electrons dominate effect was established, and the device worked as an n-n^+ junction state as shown in Figure 4 (b, iv).

To explore the photovoltaic performance of the lateral WSe_2 homojunction, the p-n diode was illumined under a laser light (λ = 530 nm) with variation in the intensity of light. A typical self-biased photovoltaic behavior is observed at the p-n junction state upon illumination of incident light, a positive open-circuit voltage (V_{oc}) is generated i.e. the voltage obtained (at I_{ds} = 0 V) and also a negative short-circuit current (I_{sc}) i.e. the current obtained (at V_{ds} = 0 V). The presence of

built-in potential in the proposed homojunction diode establishes I_{sc} and V_{oc} upon illumination, which can be implemented for a self-powered photovoltaic system in future electronics that as shown in Figure 5 (a). The identified values of the I_{sc} and V_{oc} are consistent with the lateral homojunction p-n diode and comparable to the diodes based on mix-dimensional heterostructures [61-64] or photodetectors. [65-66] The existence of a built-in potential at p-n homojunction diode established I_{sc} and V_{oc} without an external electric field, which can be implemented for a self-powered photovoltaic system in future electronics. Figure 5 (b) shows the relation between V_{oc} and I_{sc} as a function of the light intensity.

CONCLUSIONS

We established a single flake lateral WSe_2 p-n diode by photo-induced doping through optical excitation of donor-like states in a multilayered h-BN nanoflake upon illumination. This planar diode was fabricated using a dry transfer technique by stacking the WSe_2 nanoflake partially on the h-BN and Si substrate. The p-type WSe_2 nanoflake is converted to an n-type nanoflake by the photo-induced doping technique. KPFM experiments demonstrated the amendment of the Fermi level from 5.0 to 4.50 eV upon photo-induced doping. Also, the CPD across the junction of p-WSe_2 and n-WSe_2 was ~492 mV. The WSe_2 homojunction p-n diode showed a maximum rectification ratio of ~3.9×10^4 at the back gate of −30 V with the ideality factor of ~1.05. The presence of built-in potential in the proposed homojunction diode establishes I_{sc} and V_{oc} upon illumination, which can be implemented for a self-powered photovoltaic system in future electronics. This efficient photo-induced doping technique of carrier-type modulation may lead to the advancement of functional devices in the field of nanotechnology.

EXPERIMENTAL SECTION

Natural bulk crystals of h-BN and WSe_2 were bought from HQ graphene. The mechanical exfoliation technique was implemented to obtain the ultra-thin nanoflakes of h-BN and WSe_2 from their bulk form, with adhesive tape in a cleanroom environment. A dry transfer method was employed to stack the h-BN and WSe_2 heterostructures using a micromanipulator with a transparent PDMS stamp. At first, the bottom h-BN flake was dry-transferred onto SiO_2/Si substrate inside the window (90×90 μm^2) of large pattern. The top WSe_2 nanoflake was transferred by making a vertical stack i.e. WSe_2/h-BN heterostructure with the help of a micromanipulator moveable platform, we made sure that it was fit line up and partially stacked on the h-BN bottom flake and remained on the substrate. At the end of the transfer process, the substrate was placed on a hot plate at 90 °C to remove the miniature water vapors from the exterior surfaces and interfaces. Throughout the transfer process, the samples were first washed with acetone and then with methanol and dried under N_2 gas flow after each step. The heterostructures of h-BN and WSe_2 were illuminated upon the exposure to deep UV light (λ = 220 nm, 11 mW cm^{-2}). For the nanofabrication of electrodes, the regular e-beam lithography procedure was accomplished to make patterns of the source/drain electrodes. Finally, the thermal evaporation process was used to deposit the metal contacts, Pd/Au, and Al/Au with the thickness of 6/100 nm for each case on the p-WSe_2 and n-WSe_2, respectively. The WSe_2 nanoflakes were analyzed from beginning to end using optical microscopy as well as Raman spectroscopy and confirmed their thickness through atomic force microscopy (AFM). Electrical measurements were completed by placing the samples inside a vacuum box with a source meter (Keithley 2400) and Pico-ammeter (Keithley 6485). The photovoltaic measurements were done by a green laser having a wavelength of 530 nm varying the intensity of light. Commercial equipment (XE-100 and NX10 by Park System Inc.) in Kelvin

probe force microscopy (KPFM) mode was used for surface potential measurement in ambient air condition. A cantilever (NSC36) coated with Cr/Au tip was calibrated from the work function of HOPG (ϕ_{HOPG} = 4.6 eV), which is an electrically stable material, and the scan rate was 0.3 Hz. Freshly cleaved HOPG was used to calibrate the work function of the tip. The work function of HOPG is known for not changing significantly in the ambient environments, because it does not form the interface dipoles.

ASSOCIATED CONTENT

Supporting Information. The Supporting Information is available free of charge on the website. It contains Raman spectra of WSe_2 and h-BN, AFM image of h-BN/WSe_2, *I-V* characteristics of p-WSe_2 and n-WSe_2 with Pd/Au metal contacts at various V_{bg}, transfer characteristics of the h-BN/WSe_2 FET device for the photon energy of incident light, Raman spectra of pristine and doped WSe_2, transfer characteristics of n-WSe_2 after the photo-induced doping, *I-V* characteristics of p-WSe_2 with Pd/Au metal contacts, *I-V* characteristics of n-WSe_2 with Al/Au metal contacts and gate-dependent rectifying effect of the WSe_2 flake with Pd/Au and Al/Au source and drain electrodes.

Notes

The authors declare no competing financial interests.

ACKNOWLEDGEMENT

This work was supported by the Basic Science Research Program (2019R1F1A1057697) and the Global Research and Development Center Program (2018K1A4A3A01064272) through the National Research Foundation of Korea (NRF) grant funded by the Korea government (Ministry of Education and the Ministry of Science and ICT).

REFERENCES

(1) Manzeli, S.; Ovchinnikov, D.; Pasquier, D.; Yazyev, O. V.; Kis, A. 2D Transition Metal Dichalcogenides. *Nat. Rev. Mater.* **2017,** *2* (8), 17033.
(2) Aftab, S.; Eom, J. Van der Waals 2D Layered-Material Bipolar Transistor. *2D Mater.* **2019,** *6* (3), 035005.
(3) Wang, H.; Liu, F.; Fu, W.; Fang, Z.; Zhou, W.; Liu, Z. Two-Dimensional Heterostructures: Fabrication, Characterization, and Application. *Nanoscale* **2014,** *6* (21), 12250-12272.
(4) Dhanabalan, S. C.; Ponraj, J. S.; Zhang, H.; Bao, Q. Present Perspectives of Broadband Photodetectors Based on Nanobelts, Nanoribbons, Nanosheets and the Emerging 2D Materials. *Nanoscale* **2016,** *8* (12), 6410-6434.
(5) Mohsin, A.; Cross, N. G.; Liu, L.; Watanabe, K.; Taniguchi, T.; Duscher, G.; Gu, G. Mapping the Layer Count of Few-Layer Hexagonal Boron Nitride at High Lateral Spatial Resolutions. *2D Mater.* **2017,** *5* (1), 015007.
(6) Georgiou, T.; Jalil, R.; Belle, B. D.; Britnell, L.; Gorbachev, R. V.; Morozov, S. V.; Kim, Y.-J.; Gholinia, A.; Haigh, S. J.; Makarovsky, O. Vertical Field-Effect Transistor Based on Graphene–WS_2 Heterostructures for Flexible and Transparent Electronics. *Nat. Nanotechnol.* **2013,** *8* (2), 100.
(7) Kang, W.-M.; Lee, S.; Cho, I.-T.; Park, T. H.; Shin, H.; Hwang, C. S.; Lee, C.; Park, B.-G.; Lee, J.-H. Multi-Layer WSe_2 Field Effect Transistor with Improved Carrier-Injection Contact by using Oxygen Plasma Treatment. *Solid-State Electron.* **2018,** *140*, 2-7.
(8) Kang, J.; Liu, W.; Sarkar, D.; Jena, D.; Banerjee, K. Computational Study of Metal Contacts to Monolayer Transition-Metal Dichalcogenide Semiconductors. *Phys. Rev. X* **2014,** *4* (3), 031005.
(9) Li, Y.; Shi, J.; Chen, H.; Wang, R.; Mi, Y.; Zhang, C.; Du, W.; Zhang, S.; Liu, Z.; Zhang, Q. The Auger Process in Multilayer WSe_2 Crystals. *Nanoscale* **2018,** *10* (37), 17585-17592.
(10) Campbell, P. M.; Tarasov, A.; Joiner, C. A.; Tsai, M.-Y.; Pavlidis, G.; Graham, S.; Ready, W. J.; Vogel, E. M. Field-Effect Transistors Based on Wafer-Scale, Highly Uniform Few-Layer p-type WSe_2. *Nanoscale* **2016,** *8* (4), 2268-2276.
(11) Upadhyayula, L.; Loferski, J.; Wold, A.; Giriat, W.; Kershaw, R. Semiconducting Properties of Single Crystals of n‐ and p‐type Tungsten Diselenide (WSe_2). *J. Appl. Phys.* **1968,** *39* (10), 4736-4740.
(12) Frisenda, R.; Molina-Mendoza, A. J.; Mueller, T.; Castellanos-Gomez, A.; van der Zant, H. S. Atomically Thin p–n Junctions Based on Two-Dimensional Materials. *Chem. Soc. Rev.* **2018,** *47* (9), 3339-3358.
(13) Vélez, S.; Island, J.; Buscema, M.; Txoperena, O.; Parui, S.; Steele, G. A.; Casanova, F.; van der Zant, H. S.; Castellanos-Gomez, A.; Hueso, L. E. Gate-Tunable Diode and Photovoltaic Effect in an Organic–2D Layered Material p–n Junction. *Nanoscale* **2015,** *7* (37), 15442-15449.
(14) Luo, P.; Zhuge, F.; Zhang, Q.; Chen, Y.; Lv, L.; Huang, Y.; Li, H.; Zhai, T. Doping Engineering and Functionalization of Two-Dimensional Metal Chalcogenides. *Nanoscale Horiz.* **2019,** *4* (1), 26-51.
(15) Ross, J. S.; Klement, P.; Jones, A. M.; Ghimire, N. J.; Yan, J.; Mandrus, D.; Taniguchi, T.; Watanabe, K.; Kitamura, K.; Yao, W. Electrically Tunable Excitonic Light-Emitting Diodes Based on Monolayer WSe_2 p–n Junctions. *Nat. Nanotechnol.* **2014,** *9* (4), 268.

(16) Baugher, B. W.; Churchill, H. O.; Yang, Y.; Jarillo-Herrero, P. Optoelectronic Devices Based on Electrically Tunable p–n Diodes in a Monolayer Dichalcogenide. *Nat. Nanotechnol.* **2014,** *9* (4), 262.
(17) Han, C.; Hu, Z.; Gomes, L. C.; Bao, Y.; Carvalho, A.; Tan, S. J.; Lei, B.; Xiang, D.; Wu, J.; Qi, D. Surface Functionalization of Black Phosphorus via Potassium Toward High-Performance Complementary Devices. *Nano Lett.* **2017,** *17* (7), 4122-4129.
(18) Choi, M. S.; Qu, D.; Lee, D.; Liu, X.; Watanabe, K.; Taniguchi, T.; Yoo, W. J. Lateral MoS_2 p–n Junction Formed by Chemical Doping for use in High-Performance Optoelectronics. *ACS nano* **2014,** *8* (9), 9332-9340.
(19) Tang, B.; Yu, Z. G.; Huang, L.; Chai, J.; Wong, S. L.; Deng, J.; Yang, W.; Gong, H.; Wang, S.; Ang, K.-W. Direct n-to p-type Channel Conversion in Monolayer/Few-Layer WS_2 Field-Effect Transistors by Atomic Nitrogen Treatment. *ACS nano* **2018,** *12* (3), 2506-2513.
(20) Stander, N.; Huard, B.; Goldhaber-Gordon, D. Evidence for Klein Tunneling in Graphene p− n Junctions. *Phys. Rev. Lett.* **2009,** *102* (2), 026807.
(21) Ubrig, N.; Jo, S.; Berger, H.; Morpurgo, A. F.; Kuzmenko, A. B. Scanning Photocurrent Microscopy Reveals Electron-Hole Asymmetry in Ionic Liquid-Gated WS_2 Transistors. *Appl. Phys. Lett.* **2014,** *104* (17), 171112.
(22) Zhang, Y.; Ye, J.; Yomogida, Y.; Takenobu, T.; Iwasa, Y. Formation of a Stable p–n Junction in a Liquid-Gated MoS_2 Ambipolar Transistor. *Nano Lett.* **2013,** *13* (7), 3023-3028.
(23) Tosun, M.; Chuang, S.; Fang, H.; Sachid, A. B.; Hettick, M.; Lin, Y.; Zeng, Y.; Javey, A. High-Gain Inverters Based on WSe_2 Complementary Field-Effect Transistors. *ACS nano* **2014,** *8* (5), 4948-4953.
(24) Tsai, D.-S.; Liu, K.-K.; Lien, D.-H.; Tsai, M.-L.; Kang, C.-F.; Lin, C.-A.; Li, L.-J.; He, J.-H. Few-Layer MoS_2 with High Broadband Photogain and Fast Optical Switching for use in Harsh Environments. *ACS nano* **2013,** *7* (5), 3905-3911.
(25) Perera, M. M.; Lin, M.-W.; Chuang, H.-J.; Chamlagain, B. P.; Wang, C.; Tan, X.; Cheng, M. M.-C.; Tománek, D.; Zhou, Z. Improved carrier mobility in few-layer MoS2 field-effect Transistors with Ionic-Liquid Gating. *ACS nano* **2013,** *7* (5), 4449-4458.
(26) Fang, H.; Chuang, S.; Chang, T. C.; Takei, K.; Takahashi, T.; Javey, A. High-Performance Single Layered WSe_2 p-FETs with Chemically Doped Contacts. *Nano Lett.* **2012,** *12* (7), 3788-3792.
(27) Chen, B.; Sahin, H.; Suslu, A.; Ding, L.; Bertoni, M. I.; Peeters, F.; Tongay, S. Environmental Changes in $MoTe_2$ Excitonic Dynamics by Defects-Activated Molecular Interaction. *ACS nano* **2015,** *9* (5), 5326-5332.
(28) Lu, Q.; Zhao, Q.; Yang, T.; Zhai, C.; Wang, D.; Zhang, M. Preparation of Boron Nitride Nanoparticles with Oxygen Doping and a Study of their Room-Temperature Ferromagnetism. *ACS Appl. Mater. Interfaces* **2018,** *10* (15), 12947-12953.
(29) Lipp, A.; Schwetz, K. A.; Hunold, K. Hexagonal Boron Nitride: Fabrication, Properties and Applications. *J. Eur. Ceram. Soc.* **1989,** *5* (1), 3-9.
(30) Britnell, L.; Gorbachev, R. V.; Jalil, R.; Belle, B. D.; Schedin, F.; Katsnelson, M. I.; Eaves, L.; Morozov, S. V.; Mayorov, A. S.; Peres, N. M. Electron Tunneling Through Ultrathin Boron Nitride Crystalline Barriers. *Nano Lett.* **2012,** *12* (3), 1707-1710.
(31) Britnell, L.; Gorbachev, R.; Jalil, R.; Belle, B.; Schedin, F.; Mishchenko, A.; Georgiou, T.; Katsnelson, M.; Eaves, L.; Morozov, S. Field-Effect Tunneling Transistor Based on Vertical Graphene Heterostructures. *science* **2012,** *335* (6071), 947-950.

(32) Watanabe, K.; Taniguchi, T.; Kanda, H. Direct-Bandgap Properties and Evidence for Ultraviolet Lasing of Hexagonal Boron Nitride Single Crystal. *Nat. Mater.* **2004,** *3* (6), 404.
(33) Lukomskii, A.; Shipilo, V.; Gameza, L. Luminescence Properties of Graphite-Like Boron Nitride. *J. Appl. Spectrosc.* **1992,** *57* (1), 607-610.
(34) Luo, X.; Andrews, K.; Wang, T.; Bowman, A.; Zhou, Z.; Xu, Y.-Q. Reversible Photo-Induced Doping in WSe_2 Field Effect Transistors. *Nanoscale* **2019,** *11* (15), 7358-7363.
(35) Dean, C. R.; Young, A. F.; Meric, I.; Lee, C.; Wang, L.; Sorgenfrei, S.; Watanabe, K.; Taniguchi, T.; Kim, P.; Shepard, K. L. Boron Nitride Substrates for High-Quality Graphene Electronics. *J. Appl. Spectrosc.* **2010,** *5* (10), 722.
(36) Zomer, P.; Dash, S.; Tombros, N.; Van Wees, B. A Transfer Technique for High Mobility Graphene Devices on Commercially Available Hexagonal Boron Nitride. *Appl. Phys. Lett.* **2011,** *99* (23), 232104.
(37) Wu, Z.; Hong, J.; Jiang, J.; Zheng, P.; Zheng, L.; Ni, Z.; Zhang, Y. Photoinduced Doping in Monolayer WSe_2 Transistors. *Appl. Phys. Express* **2019,** *12* (9), 094005.
(38) Nipane, A.; Karmakar, D.; Kaushik, N.; Karande, S.; Lodha, S. Few-Layer MoS_2 p-type Devices Enabled by Selective Doping using Low Energy Phosphorus Implantation. *ACS nano* **2016,** *10* (2), 2128-2137.
(39) Ju, L.; Velasco Jr, J.; Huang, E.; Kahn, S.; Nosiglia, C.; Tsai, H.-Z.; Yang, W.; Taniguchi, T.; Watanabe, K.; Zhang, Y. Photoinduced Doping in Heterostructures of Graphene and Boron Nitride. *Nat. Nanotechnol.* **2014,** *9* (5), 348.
(40) Lim, J. Y.; Pezeshki, A.; Oh, S.; Kim, J. S.; Lee, Y. T.; Yu, S.; Hwang, D. K.; Lee, G. H.; Choi, H. J.; Im, S. Homogeneous 2D $MoTe_2$ p‐n Junctions and CMOS Inverters Formed by Atomic‐Layer‐Deposition‐Induced Doping. *Adv. Mater.* **2017,** *29* (30), 1701798.
(41) Luo, W.; Zhu, M.; Peng, G.; Zheng, X.; Miao, F.; Bai, S.; Zhang, X. A.; Qin, S. Carrier Modulation of Ambipolar Few‐Layer MoTe2 Transistors by MgO Surface Charge Transfer Doping. *Adv. Funct. Mater.* **2018,** *28* (15), 1704539.
(42) Ross, J. S.; Klement, P.; Jones, A. M.; Ghimire, N. J.; Yan, J.; Mandrus, D. G.; Taniguchi, T.; Watanabe, K.; Kitamura, K.; Yao, W.; Cobden, D. H.; Xu, X. Electrically Tunable Excitonic Light-Emitting Diodes Based on Monolayer WSe_2 p–n Junctions. *Nat. Nanotechnol.* **2014,** *9*, 268, DOI: 10.1038/nnano.2014.26
https://www.nature.com/articles/nnano.2014.26#supplementary-information.
(43) Wang, J.; Ma, F.; Sun, M. Graphene, Hexagonal Boron Nitride, and their Heterostructures: Properties and Applications. *RSC Adv.* **2017,** *7* (27), 16801-16822.
(44) Aftab, S.; Iqbal, M. W.; Afzal, A. M.; Khan, M. F.; Hussain, G.; Waheed, H. S.; Kamran, M. A. Formation of an $MoTe_2$ based Schottky Junction Employing Ultra-Low and High Resistive Metal Contacts. *RSC Adv.* **2019,** *9* (18), 10017-10023.
(45) Yu, X.; Zhang, S.; Zeng, H.; Wang, Q. J. Lateral Black Phosphorene P–N Junctions Formed via Chemical Doping for High Performance Near-Infrared Photodetector. *Nano Energy* **2016,** *25*, 34-41.
(46) Jin, Y.; Keum, D. H.; An, S. J.; Kim, J.; Lee, H. S.; Lee, Y. H. A Van Der Waals Homojunction: Ideal p–n Diode Behavior in $MoSe_2$. *Adv. Mater.* **2015,** *27* (37), 5534-5540.
(47) Iqbal, M.; Firdous, F.; Manzoor, M.; Ateeq, H.; Azam, S.; Aftab, S.; Kamran, M.; ul Rehman, A.; Majid, A. Study of Electrical Attributes of Molybdenum Ditelluride (MoTe2) FET using Experimental and Theoretical Evidences. *Microelectron. Eng.* **2020**, 230, 111365.

(48) Wu, E.; Xie, Y.; Zhang, J.; Zhang, H.; Hu, X.; Liu, J.; Zhou, C.; Zhang, D. Dynamically Controllable Polarity Modulation of $MoTe_2$ Field-Effect Transistors through Ultraviolet Light and Electrostatic Activation. *Sci. Adv.* **2019,** *5* (5), eaav3430.
(49) Tosun, M.; Chan, L.; Amani, M.; Roy, T.; Ahn, G. H.; Taheri, P.; Carraro, C.; Ager, J. W.; Maboudian, R.; Javey, A. Air-Stable n-doping of WSe_2 by Anion Vacancy Formation with Mild Plasma Treatment. *ACS nano* **2016,** *10* (7), 6853-6860.
(50) Stanford, M. G.; Pudasaini, P. R.; Belianinov, A.; Cross, N.; Noh, J. H.; Koehler, M. R.; Mandrus, D. G.; Duscher, G.; Rondinone, A. J.; Ivanov, I. N. Focused Helium-Ion Beam Irradiation Effects on Electrical Transport Properties of Few-Layer WSe_2: Enabling Nanoscale Direct write Homo-Junctions. *Sci. Rep.* **2016,** *6*, 27276.
(51) Aftab, S.; Khan, M. F.; Gautam, P.; Noh, H.; Eom, J. $MoTe_2$ Van der Waals Homojunction p–n Diode with Low Resistance Metal Contacts. *Nanoscale* **2019**, *11*(19), 9518-9525.
(52) Pan, Y.; Li, S.; Ye, M.; Quhe, R.; Song, Z.; Wang, Y.; Zheng, J.; Pan, F.; Guo, W.; Yang, J. Interfacial Properties of Monolayer $MoSe_2$–Metal Contacts. *J. Phys. Chem. C* **2016,** *120* (24), 13063-13070.
(53) Iqbal, M. W.; Iqbal, M. Z.; Khan, M. F.; Shehzad, M. A.; Seo, Y.; Park, J. H.; Hwang, C.; Eom, J. High-Mobility and Air-Stable Single-Layer WS_2 Field-Effect Transistors Sandwiched Between Chemical Vapor Deposition-Grown Hexagonal BN Films. *Sci. Rep.* **2015,** *5*, 10699.
(54) Reuter, C.; Frisenda, R.; Lin, D. Y.; Ko, T. S.; Perez de Lara, D.; Castellanos‐Gomez, A. A Versatile Scanning Photocurrent Mapping System to Characterize Optoelectronic Devices Based on 2D Materials. *Small Methods* **2017,** *1* (7), 1700119.
(55) Liu, Y.; Cai, Y.; Zhang, G.; Zhang, Y. W.; Ang, K. W. Al‐Doped Black Phosphorus p‐n Homojunction Diode for High Performance Photovoltaic. *Adv. Funct. Mater.* **2017,** *27* (7), 1604638.
(56) Buscema, M.; Groenendijk, D. J.; Blanter, S. I.; Steele, G. A.; Van Der Zant, H. S.; Castellanos-Gomez, A. Fast and Broadband Photoresponse of Few-Layer Black Phosphorus Field-Effect Transistors. *Nano Lett.* **2014,** *14* (6), 3347-3352.
(57) Pospischil, A.; Furchi, M. M.; Mueller, T. Solar-Energy Conversion and Light Emission in an Atomic Monolayer p–n Diode. *Nat. Nanotechnol.* **2014,** *9* (4), 257-261.
(58) Li, H.-M.; Lee, D.; Qu, D.; Liu, X.; Ryu, J.; Seabaugh, A.; Yoo, W. J. Ultimate Thin Vertical p–n Junction Composed of Two-Dimensional Layered Molybdenum Disulfide. *Nat. Commun.* **2015,** *6* (1), 1-9.
(59) Dhyani, V.; Das, S. High-Speed Scalable Silicon-MoS_2 PN Heterojunction Photodetectors. *Sci. Rep.* **2017,** *7*, 44243.
(60) Gehring, P.; Urcuyo, R.; Duong, D. L.; Burghard, M.; Kern, K. Thin-Layer Black Phosphorus/GaAs Heterojunction pn Diodes. *Appl. Phys. Lett.* **2015,** *106* (23), 233110.
(61) Riazimehr, S.; Schneider, D.; Yim, C.; Kataria, S.; Passi, V.; Bablich, A.; Duesberg, G. S.; Lemme, M. C. In *Spectral Sensitivity of a Graphene/Silicon pn-Junction Photodetector*, EUROSOI-ULIS 2015: 2015 Joint International EUROSOI Workshop and International Conference on Ultimate Integration on Silicon, IEEE: 2015; pp 77-80.
(62) Chowdhury, R. K.; Maiti, R.; Ghorai, A.; Midya, A.; Ray, S. K. Novel Silicon Compatible p-WS_2 2D/3D Heterojunction Devices Exhibiting Broadband Photoresponse and Superior Detectivity. *Nanoscale* **2016,** *8* (27), 13429-13436.
(63) Yu, Y.; Fong, P. W.; Wang, S.; Surya, C. Fabrication of WS_2/GaN pn Junction by Wafer-Scale WS_2 Thin Film Transfer. *Sci. Rep.* **2016,** *6*, 37833.

(64) He, L.; Xiu, F.; Wang, Y.; Fedorov, A. V.; Huang, G.; Kou, X.; Lang, M.; Beyermann, W. P.; Zou, J.; Wang, K. L. Epitaxial Growth of Bi_2Se_3 Topological Insulator Thin Films on Si (111). *J. Appl. Phys.* **2011,** *109* (10), 103702.
(65) Zheng, Z.; Zhang, T.; Yao, J.; Zhang, Y.; Xu, J.; Yang, G. Flexible, Transparent and Ultra-Broadband Photodetector Based on Large-Area WSe_2 Film for Wearable Devices. *Nanotechnology* **2016,** *27* (22), 225501.
(66) Zhang, W.; Chiu, M.-H.; Chen, C.-H.; Chen, W.; Li, L.-J.; Wee, A. T. S. Role of Metal Contacts in High-Performance Phototransistors Based on WSe_2 Monolayers. *ACS nano* **2014,** *8* (8), 8653-8661.

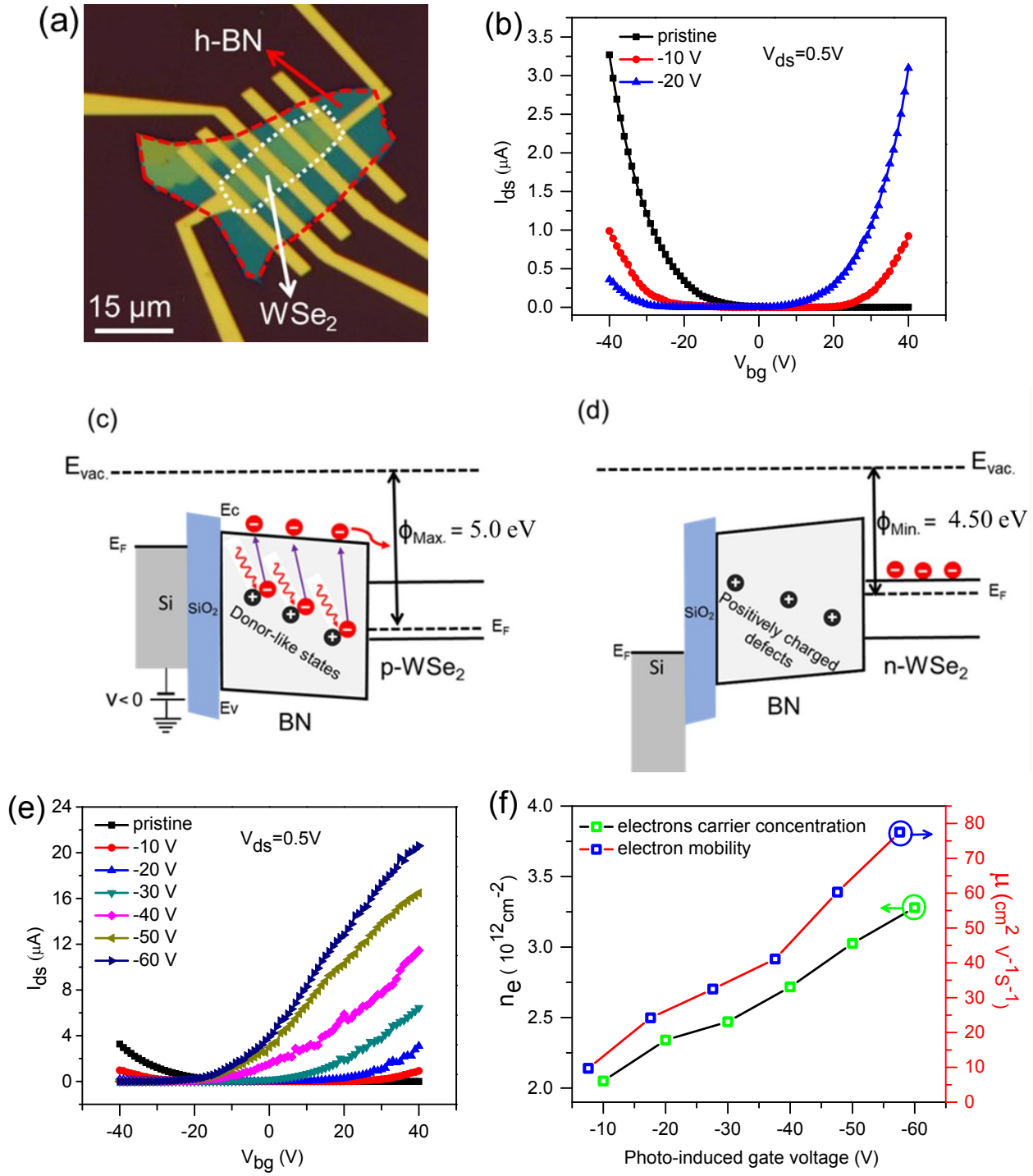

Figure 1. (a) Optical image of an h-BN/WSe_2 FET. (b) The transfer characteristics of pristine and doped h-BN/WSe_2 FET device with a light pulse of 5 minutes. The energy of incident photons is 5.6 eV. (c) The schematic of photo-induced doping mechanism, where incident light excites electrons from defect states in the h-BN. The excited electrons can enter into the WSe_2 flake under

V_g^{light}. (d) The donor-like states in the middle of h-BN become positively charged defects after the photo-induced doping at V_g^{light}. (e) Transfer characteristics of the h-BN/WSe_2 FET device after photo-induced doping at V_g^{light} for 5 minutes of illumination. (f) The plot of electron mobility (μ) and electron carrier concentration (n_e) as a function of V_g^{light}.

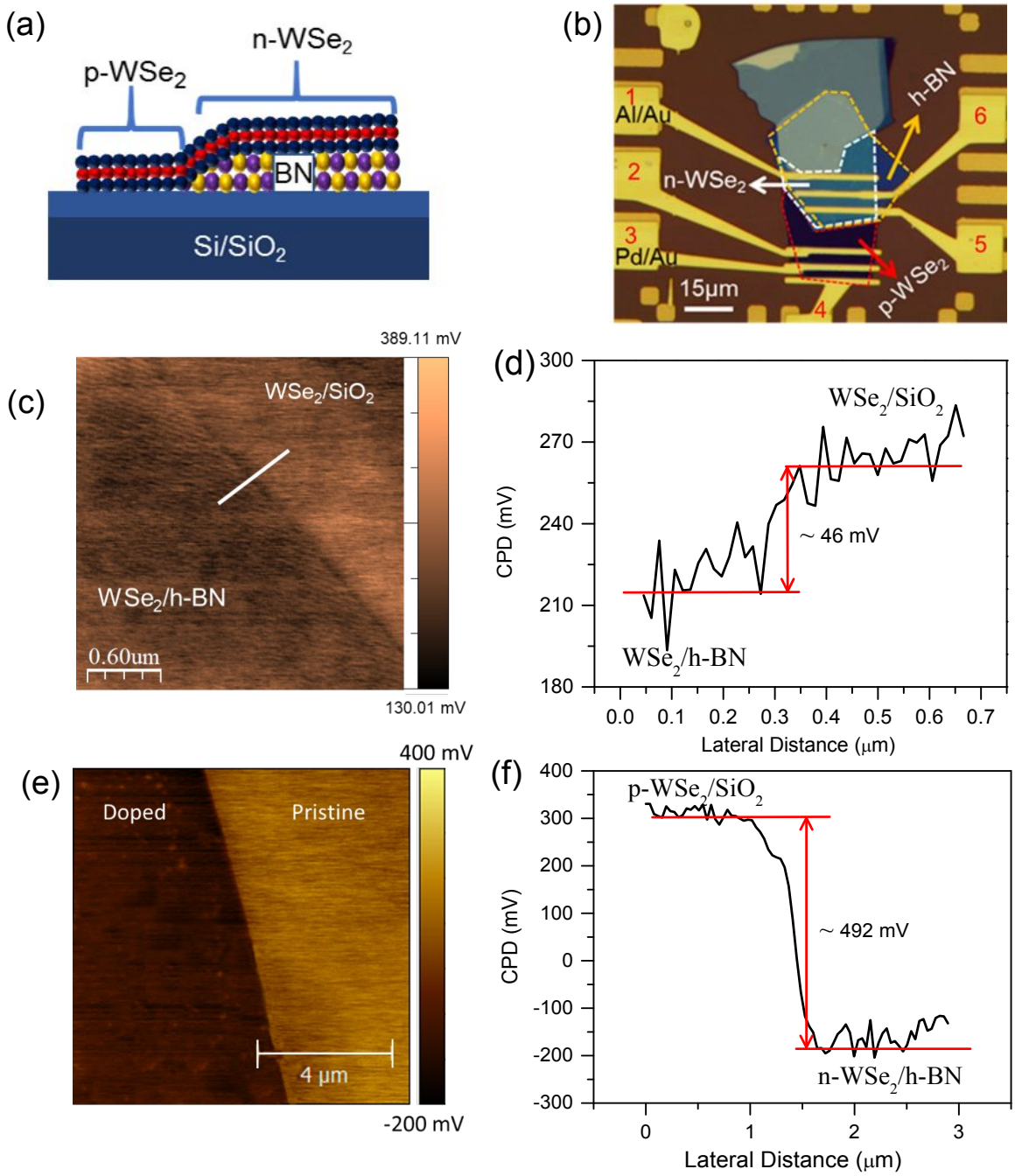

Figure 2. (a) An illustration of the lateral WSe_2 p–n diode. (b) The optical image of WSe_2 homojunction p-n diode. (c) KPFM image of the WSe_2 flake before the doping process. (d) The corresponding step height profile from the KPFM line scan is indicated. The value of contact potential difference across WSe_2/h-BN and WSe_2/ SiO_2 is approximately ~46 mV. (e) A KPFM image of the WSe_2 flake for doped and undoped regions at a $V_g^{light} =$ −40 V. (f) The corresponding step height profile from the KPFM line scan is indicated. The value of the contact potential difference across h-BN/n-WSe_2 and SiO_2/p-WSe_2 is approximately ~492 mV.

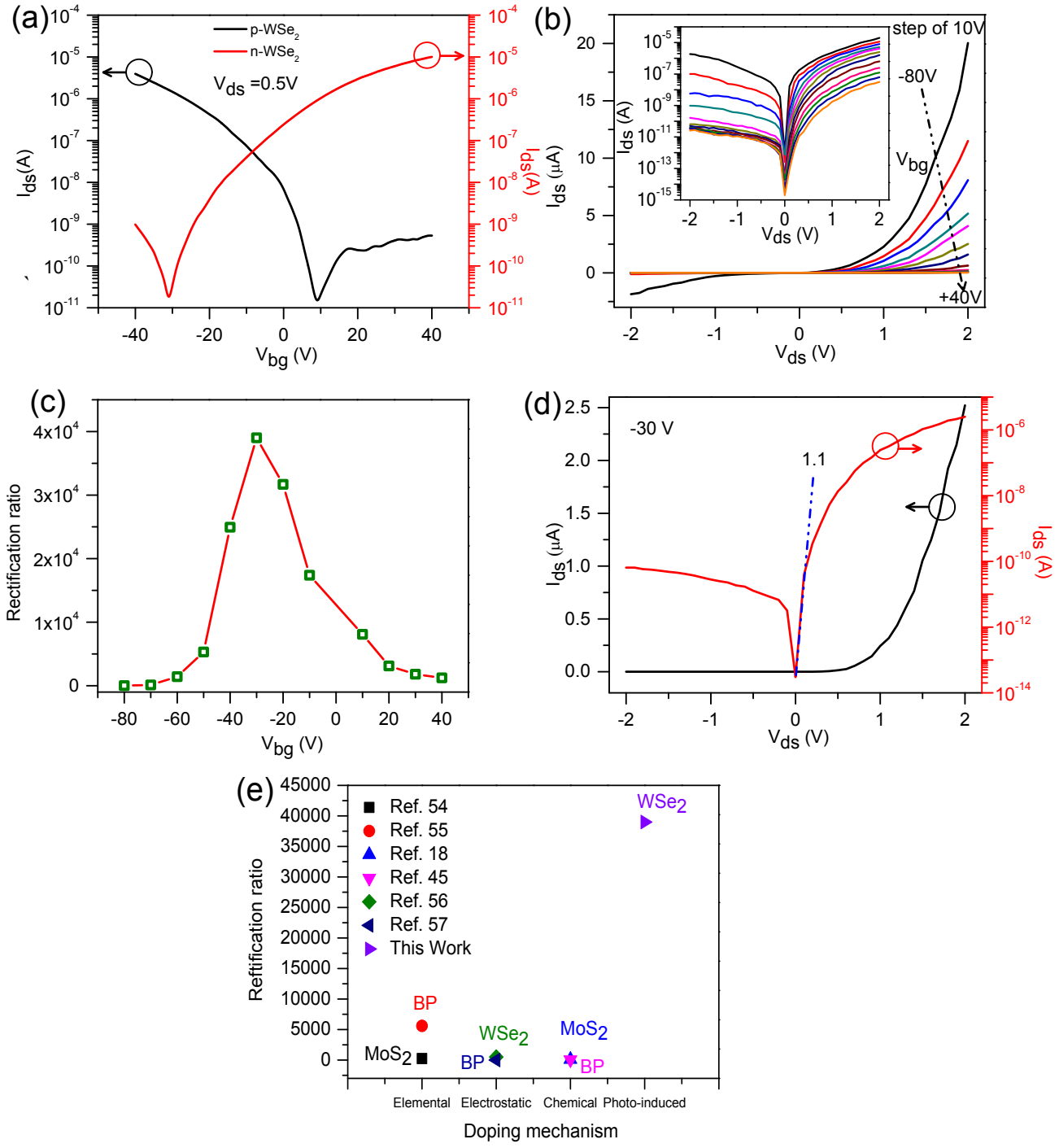

Figure 3. (a) Transfer curves of p-WSe_2 from probe (2, 3) and n-WSe_2 from probe (1, 6) as a function of V_{bg}. (b) Gate-dependent rectifying effect of the WSe_2 homojunction p-n diode with probe (5, 2) in a linear scale. Inset of (d) shown in log scale. (c) The rectification ratio of WSe_2 homojunction p-n diode as a function back gate voltage (V_{bg}). (d) The ideality factor of the device at $V_{bg} = -30$ V. (e) Rectification ratio as a function of different doping mechanisms in 2D materials.

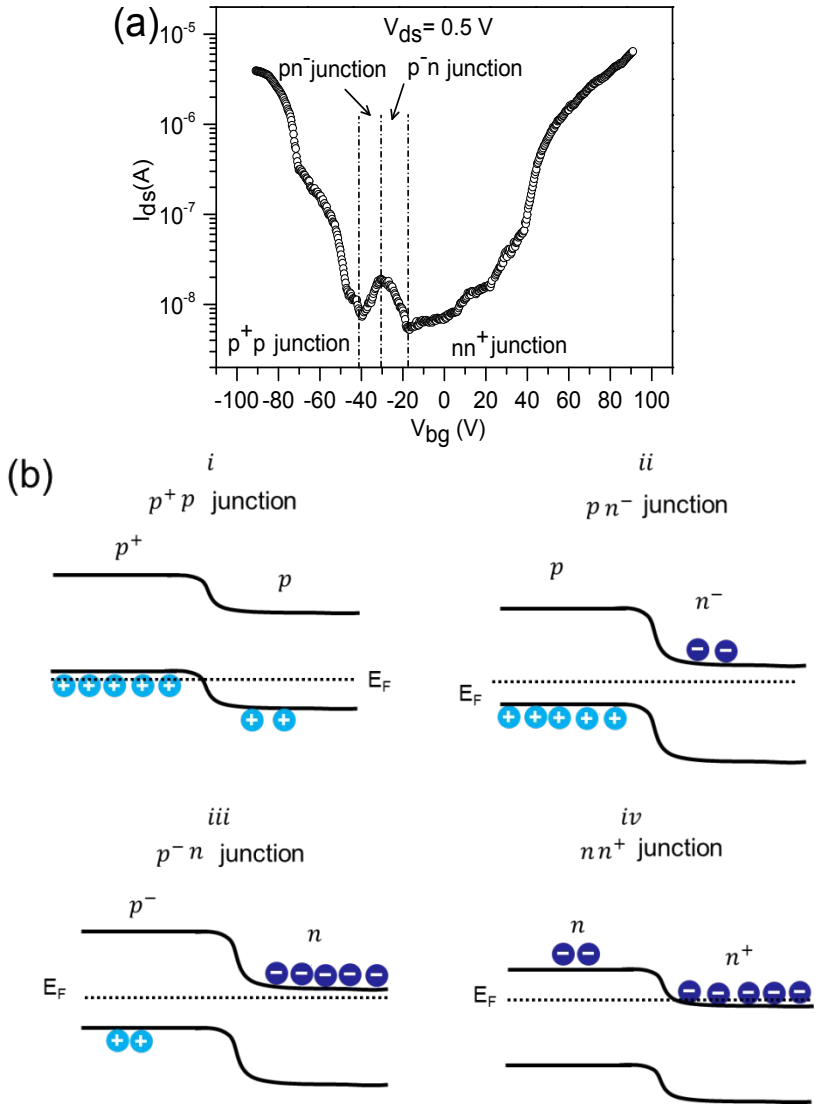

Figure 4. (a) Transfer characteristics of the WSe_2 diode with probe (5, 2) for four doping regimes as a function of back gate voltage (V_{bg}). (b) Energy band diagram showing four different junctions with tuning the back gate.

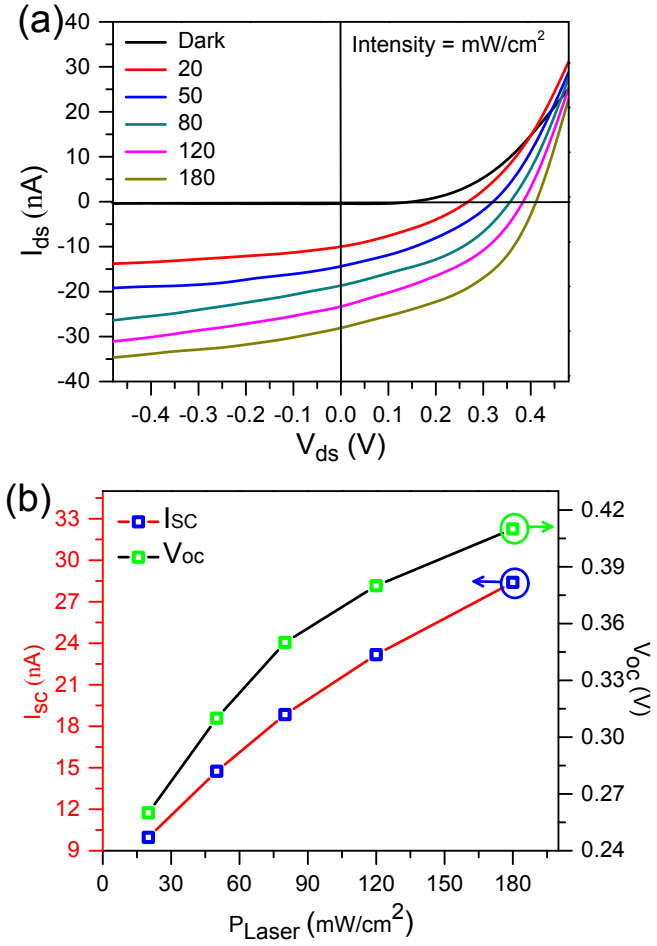

Figure 5. (a) I_D-V_D characteristics of the device under dark and light illumination at V_{bg}= 0 V. (b) The open circuit voltage (V_{oc}) and short circuit current (I_{sc}) is shown as a function laser power.

TOC

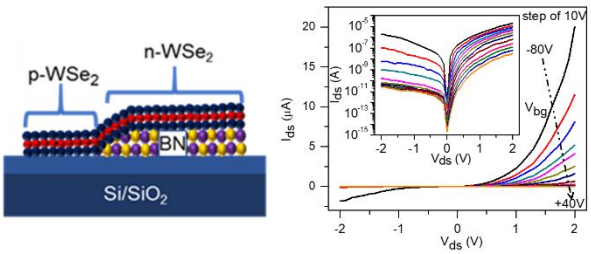
p-WSe2
n-WSe2
BN
Si/SiO2
step of 10V
-80V
Vbg
+40V
Ids (μA)
Vds (V)
Ids (A)
Vds (V)